Structural, Magnetic Properties and Hyperthermia Efficiency of MF/$CuAl_2O_4$ Multiferroic Nanocomposite

Roumaih Roumaih (khroumaih@yahoo.com)
Nuclear Research Center, Egyptian Atomic Energy Authority https://orcid.org/0000-0003-3018-8545
Ismail Abd-elrahem
Nuclear Research Center, Egyptian Atomic Energy Authority
Shaban I. Hussein
Nuclear Research Center, Egyptian Atomic Energy Authority

Research Article

Keywords: Multiferroic materials, Spinel ferrite, Magnetic susceptibility, SAR.

Posted Date: September 1st, 2021

DOI: https://doi.org/10.21203/rs.3.rs-851259/v1

Version of Record: A version of this preprint was published at Chinese Journal of Physics on March 1st, 2022. See the published version at https://doi.org/10.1016/j.cjph.2022.03.009.

Abstract

The multiferroic MF/$CuAl_2O_4$ (MF= $CoFe_2O_4$, $NiFe_2O_4$, $MgFe_2O_4$, and $ZnFe_2O_4$) was prepared using two stages of the sol-gel method. X-ray Diffraction (XRD), the Fourier transforms infrared absorption (FT-IR) and High-resolution Transmission Electron Microscope (HR-TEM) were used to examine the structure of all samples. From the XRD patterns, two standards of cubic spinels structure ($CuAl_2O_4$ + MF) were observed. The analysis of FTIR spectra confirmed the formation of the chemical and molecular structure changes in the MF/$CuAl_2O_4$. HR-TEM images showed a uniform particle distribution with a nanoscale of all samples. The magnetic properties were studied from the hysteresis loops using a vibrating sample magnetometer (VSM) and the magnetization M (T) by the Faraday balance method. All samples exhibited typical ferrimagnetic behavior, except for ZnF/CuAl recorded superparamagnetic. Curie temperature (T_C) for all nanocomposites obtained from M(T) protocols, which is lower than the standard value of MF nanoferrites. The heating efficiency of all samples was investigated by measuring the Specific Absorption Rate (SAR) parameter. The SAR of NiF/CuAl showed a maximum value as well as saturation magnetization (M_s) and lowest coercivity (H_c) value.

1. Introduction

Ferrites materials are the most sensitive to magnetism, which can be controlled from the outside. Therefore it can be bound by cancer cells inside the body for early diagnosis of cancer. Nanoferrite materials with helpful magnetic properties can be incorporated into tumor tissues due to their small size. Then, an oscillating magnetic field can be applied so that magnetic nanoparticles interact with this field to generate heat and destroy cancer cells (the so-called hyperthermia). Many studies [1-8] consider, in detail, different aspects of thermal therapies of cancer diseases. The application of magnetic nanoferrites in medicine is possible due to their ability to heat up under the influence of a variable magnetic field because of the different types of thermal losses (eddy currents, magnetization reversal losses, and mechanical rotation of nanoparticles).

The combination of two components with different physical properties leads to forming a new material with improved and useful properties and eliminated the disadvantages of each material compared to its components [9, 10]. In this work, the multiferroic MF/CuAl synthesizes as a brand-new classification of nanocomposites. Because it is a combination of two materials, one of them is magnetic (soft or hard), and the other is nonmagnetic The structure of MF/CuAl nanocomposites may be able to improve the magnetic properties of MF ferrites. Besides, the distinct values of the magnetic properties of these MF ferrites allow investigating the main interactions between them. The $CoFe_2O_4$ nanoferrites possess large magnetocrystalline anisotropy and a hard-magnetic behavior originates [11]. On the other hand, the nanoferrites $NiFe_2O_4$ [12], and $MgFe_2O_4$ [13] are soft-magnetic behavior having minimum coercivity, whereas the nano ferrite $ZnFe_2O_4$ [13] have superparamagnetic behavior.

Our goal is to synthesize very distinct samples that have new magnetic properties and the hyperthermia phenomenon. So the strategy of this work will be to synthesize the multiferroic MF/$CuAl_2O_4$ (MF= $CoFe_2O_4$, $NiFe_2O_4$, $MgFe_2O_4$, and $ZnFe_2O_4$) as a brand-new classification of nanocomposites. Then, the magnetic properties and the hyperthermia of all nanocomposites were studied. This study is important for various biological and medical applications such as contrast-enhanced magnetic resonance imaging, hyperthermia of pathological tissues, controlled drug release, and separation of nucleic acids.

2. Experimental Details

2.1 Synthesis of MF/CuAl

The multiferroic MF/CuAl was prepared by the seed and the growth method, so two steps must be done. The first step was the preparation of the seed (CuAl). The preparation and characterization of the seed (CuAl) nanoparticles were published in previous work [14]. Then, the second is the growing of MF nanoferrites on the seed (CuAl). The stoichiometric weights of ferric nitrate $Fe(NO_3)_3{\cdot}9H_2O$ and nickel nitrate $Ni(NO_3)_2.6H_2O$ were dispersed in de-ionized water, individually then the solutions were mixed and then added 1.5 gm of CuAl nanoparticle to the mixture. The mixture was stirred for 120 min at room temperature at a magnetic stirrer constant speed. The citric acid ($C_6H_8O_7.H_2O$) solution was added to the mixture solution, keeping constant stirring. Then added dropwise of the ammonia solution to the mixture solution until the pH reached 7. The mixture solution was heated on a hot plate, forming a green-brown gel which decomposed by spontaneous self-ignition to foaming, and puffing, leaving behind a voluminous green-brown powder. The final powder of $NiFe_2O_4$/$CuAl_2O_4$ (NiF/CuAl) was left on a hot plate for two h to dry. The same steps were followed to prepare the other nanocomposites $CoFe_2O_4$/$CuAl_2O_4$ (CoF/CuAl), $MgFe_2O_4$/$CuAl_2O_4$ (MgF/CuAl), and $ZnFe_2O_4$/$CuAl_2O_4$ (ZnF/CuAl). The weight ratios of $NiFe_2O_4$, $CoFe_2O_4$, $MgFe_2O_4$, and $ZnFe_2O_4$ to $CuAl_2O_4$ » 2.5:1 respectively. The final powders for all nanocomposites MF/CuAl were ground manually using agate mortar.

2.2 Characterization

In this work, all experiments were performed on all samples as-prepared. Using a Philips X'pert diffractometer with CuKa radiation and wavelength l = 0.154 nm for XRD measurements. The XRD spectra were analyzed using Rietveld's refinement method employing the MAUD program [15]. The goodness of the refinement of the structure is reached if the S parameter » 1.0.

The FTIR spectrum was recorded in the wavenumber range of 4000–400 cm^{-1}, using an FTIR spectrometer (Perkin Elmer, Spectrum 100, USA).

A Faraday balance is a device for measuring magnetic susceptibility. In this technique, the sample is suspended between electromagnet cores where a magnetic field is applied. Then, the sample is heated gradually using a non-inductive furnace. After measuring the pull of the balance (**Δm**), many parameters

can be calculated such as the molar magnetic susceptibility (χ_m), and the molar magnetization (M_m) can be calculated using the following relations respectively:

$$c_m = [(\Delta m \times g \times M_W)] / [m \times H \times (dH/dZ)] \quad (1)$$

$$M_m = \chi_m \times H \quad (2)$$

where: **g** is the gravity = 980.6 cm/s^2, M_w is the molecular weight of the sample, ***m*** is the mass of the sample, **H** is the magnetizing field applied (1300 Gs), **dH/dZ** is the magnetic field gradient in the z-direction. The magnetic ordering temperature was determined from room temperature to 750 K, using Faraday's method under a magnetic field of 130 mT.

The magnetic behavior of the prepared samples was investigated at room temperature using Vibrating Sample Magnetometer (VSM) (type: LakeShore 7410). To evaluate the heat efficacy of the sample with the alternating magnetic field, a suspended solution of MF samples was prepared according to Ref. [10]. The suspension was contained in a Pyrex tube placed in the center of the copper induction coil (type DW-UHF-10 kW) with external field H =9.27 kAm^{-1} and frequency = 198 kHz. The temperature values versus the time were registered using a red alcohol thermometer and stopwatch with polymer isolation to avoid any interfering effect of the eternal temperature.

3. Results And Discussions

3.1 Structural properties

Fig. 1 shows the XRD spectra of the CuAl and MF/CuAl samples. The XRD confirms a pure double spinel cubic structure for CuAl with MF without any undesired impurity peaks. It indicates that the seed/growth method success of preparation CuAl/MF structure. From the pattern of XRD, one can see that it is holding two spinel phases as follows: Double peaks side by side at particular positions as depicted in Fig. 1. Where the peaks located at the lower angles correspond to MF, but those at the higher correspond to CuAl, so the lattice constant of MF is higher than the CuAl as mentioned in Table 1. Moreover, a broadening of the peaks of all samples indicating that all samples have a small particle size. The structural parameters (lattice parameter ***a*** (Å), and crystallite size (*D*)) of MF and CuAl were compared with the Crystallography Open Database (COD) and tabulated in Table 1. In particularly, by considering the ionic radii of the metal ions Zn^{2+} (0.60 Å), Co^{2+} (0.58 Å), Mg^{2+} (0.57 Å) and Ni^{2+} (0.55 Å) [16], the lattice parameters of MF increased with the ionic radii as 8.443 Å for ZnF, 8.385 Å for CoF, 8.376 Å for MgF and 8.373 Å for NiF. From Table 2 notice that the lattice parameter of CuAl (8.074-8.089 Å) is varied according to MF, but it matches with the previous work [13]. Besides the lattice parameter of CoF, MgF, and ZnF is slightly decreased compared to the literature [17-20], but the NiF is increasing comparable to Ref. [19]. In other words, the lattice of ZnF, MgF, and CoF is compressed after mixing, but the NiF is expanded. It is indicated that there is an interaction force between the MF and CuAl affecting the crystal structure and the other properties of all nanocomposites under investigation. This behavior can be explained by the redistribution

of the ions within the interstitial sites (A, and B-sites) according to the force between MF and CuAl, which caused changes in their properties [21]. The change in the lattice parameter of MF nanocomposites may be attributed to the degree of inversion [22].

The crystallites size obtained from Rietveld of all nanocomposites MF/CuAl was in the nanoscale (Table 1). Again, the value of the crystallites size of CuAl is dependent on the second phase, which differs from the previously reported (31 nm) [13]. Furthermore, it is noticed that the phase concentration (***%***) of all nanocomposites MF/CuAl was slightly compared to the preparation weight ratios.

3.2 Micro-Structural properties

Fig. 2 shows the TEM images of the MF/CuAl nanocomposites, with an inserted particle size histogram. The images confirm the formation of nanostructured composite with more than one grain size, indicating that there is more than one phase. The grains seem to be loose aggregates which are different slightly comparable to the particle size obtained by XRD. Although the XRD determines each lattice of MF/CuAl individually, the TEM recognizes the MF/CuAl as one compound. The average grain size (***Z*** nm) of all nanocomposites was calculated and tabulated in Table 1. For the ZnF/CuAl nanocomposite, it is observed long nanotubes with a diameter of 12 nm besides some nanograins shown in Fig. 3. The obtained nanotube is dependent on the growth mechanism of the $ZnFe_2O_4$, as reported in the literature [23, 24].

3.3 FT-IR analysis

The FT-IR absorption spectroscopy was used to study the distribution of ions at the tetrahedral sites (n_T) and octahedral sites (n_O) of spinel structure [25]. The band (n_T) and the band (n_O) were obtained from the stretching vibration of the unit cell in the A-site, and the metal-oxygen vibration in the B-site, respectively [26]. In this work, the only band obtained at absorption range 550 - 520 cm^{-1} for the tetrahedral (n_T), because the start point of the FT-IR spectroscopy was 400 cm^{-1}, so the octahedral band (n_O) was disappeared. Here, we will try to deconflict the interference between the peaks of CuAl and MF at (n_T). Besides, the force constants of the ferrite systems will calculate. Fig. 4 shows the measured IR spectra of the MF/CuAl nanocomposite samples, and the absorption peak wavelengths are listed in Table 3. It is observed that the n_t band of ZnF/CuAl recorded the lowest value in the wavenumber position while small shifts were observed with MgF/CuAl, CoF/CuAl, and NiF/CuAl towards higher wavenumbers. This indicates the strengthening of the metal-oxygen bonds at the tetrahedral sites due to the presence of Zn, the heaviest in mass, and the light shit is due to the presence of Fe ion in the others in the tetrahedral sites. This behavior agrees with the results of the Cu-Zn mixed ferrites [27].In other words, the changing in the mass ions on the tetrahedral (A) site causes a shift that increases the (A-O) bond length at the tetrahedral site of spinel structure (i.e. decrease in n_t band).

The changing in the v_T position of the MF/CuAl could be interpreted from four parameters: the 1^{st} is the total mass of cations, the $2^{nd,}$ and 3^{rd} are the length and strength of the metal-oxygen bond respectively,

and the 4th is the dimension of the unit cell. These parameters may compete with each other and cause a change in the ion position. All these parameters impact the position of the IR bands through the relation [28]:

$$v = 1307\sqrt{\frac{k}{m}} \quad (3)$$

where *k* is the force constant and *m* the atomic mass of the metal. The values of the force constant for tetrahedral (k_T) sites are listed in Table 3.

3.4 Magnetic properties

The magnetic behavior of the MF/CuAl nanocomposites varies according to the magnetic moments of Ni^{2+}, Co^{2+}, Mg^{2+}, and Zn^{2+} ions which have 2.3 mB, 3.9 mB, 0 mB, and 0 mB, respectively. To investigate the magnetic properties of the MF/CuAl nanocomposites, we measured the temperature dependence of magnetic susceptibility curves, i.e. c-T, and the applied magnetic field dependence of magnetization curves, i.e., M-H curve. Also, the heating efficiency (SAR) was determined.

3.4.1 Magnetic susceptibility

The Curie temperature (T_C) is an essential magnetic property and is considered a compositional-dependent parameter. The measured M-T curve of the MF/CuAl nanocomposites is shown in Fig. 5. The T_C is derived from the peak of $dc_m(T)/dT$ and the T_C values are tabulated in Table 4. With increasing temperature, a smoothly drop-in magnetic susceptibility occurred. In other words, the smooth transition from ferrimagnetic to paramagnetic at the T_C can be used as a measure of the degree of compositional homogeneity in all samples [29]. The T_C for NiF/CuAl, CoF/CuAl, and the MgF/CuAl is 561 K, 462 K, and 438K respectively, which is lower than the NiF 0(865 K) [30], CoF (677 K) [22], and MgF (648K) [31]. This may be due to the influence of the grain size and the cation distribution of the A- and B-sites. The transition temperature can be explained by the finite scaling theory [30]. When the grain sizes are smaller, the transition temperature is lower. Furthermore, the mutual effect between MF and $CuAl_2O_4$ leads to a lower magnetic transition temperature. The same behavior was observed in the many compounds of nanoparticles [32-34].

Figure 6 shows the relation between the reciprocal magnetic susceptibility (c_M^{-1}) and the temperature (T) for NiF/CuAl, CoF/CuAl, and MgF/CuAl samples. The relation obeyed the well-known Curie-Weiss law in the paramagnetic region. So the experimental effective magnetic moments m_{eff} and the Curie Weiss constant (Θ) values can be calculated from the plot of c_M^{-1} versus T using the relation:

$$m_{eff} = 2.82787\sqrt{C} \quad (4)$$

where C is the Curie constant equal to the slope of the line in the paramagnetic region and presented in Table 4. The Curie Weiss constant (Θ) values are equal to the cross of the slope with the x-axis in Fig. 6 and listed in Table 4. The Curie-Weiss constant (Θ) was found to possess large +ve values pointing to perfect ferrimagnetic character. The rise in Θ values assures the enhanced ferrimagnetic order of the NiF/CuAl, CoF/CuAl, and MgF/CuAl. This indicates these samples have magnetic ferrimagnetic ordering in the temperature range 300-600K. Also, the values of the Curie Weiss constant (Θ) for all samples are closed to the values of the Curie temperature of the magnetization (T_C).

3.4.2 Magnetic hysteresis loops

Fig. 7 shows the hysteresis loops for the MF/CuAl nanocomposites at room temperature. The MF/CuAl nanocomposites exhibit a ferromagnetic behavior, except the ZnF/CuAl records a superparamagnetic one. It indicates the order of magnetic structure due to the presence of the ferrite material CoF, NiF, and MgF. The estimated values of saturation magnetization (M_s), remnant magnetization (M_r), and coercive field (H_c) of the nanocomposites were listed in Table 4. As expected, the values of (M_s) are different according to the multi-phase nanocomposite. One can notice that the magnetization values of NiF/CuAl and MgF/CuAl nanocomposites are less than that of CoF/CuAl nanocomposite, where the CoF nanoferrite is hard-magnetic, i.e., large magnetocrystalline anisotropy, while NiF and MgF are soft type nanoferrites. The magnetic properties are affected by the degree of magnetic phase dispersion in the Nanocomposites i.e., the mutual effect between MF and $CuAl_2O_4$; this effect appears in the magnetic properties. As shown in Table 4, the saturation magnetization of the MF/CuAl nanocomposites is lower than the standard value of MF nanoferrites; $CoFe_2O_4$ ($M_s \approx$ 52-54 emu/g) [8], $NiFe_2O_4$ ($M_S \approx$ 50 emu/g) [12, 35], and $MgFe_2O_4$ ($M_s \approx$ 14.6 emu/g) [12, 36]. This result means that the effect of $CuAl_2O_4$ on the magnetic moment of CoF, NiF, and MgF is negative, i.e., the net magnetic moment of MF/CuAl reduced. But for ZnF/CuAl the situation is different, the ideal behavior of bulk ZnF ferrite recorded with normal spinel structure, where all Zn^{2+} ions occupy A sites and Fe^{3+} ions occupying B sites, it is antiferromagnetic. At the nanoscale, the ZnF has a partial inverse spinel structure and ferrimagnetic behavior ($M_s \approx$ 5.7 emu/g) [37, 38]. In our work, the ZnF/CuAl nanocomposite is superparamagnetic behavior as in the inset of Fig. 7, which agrees with the loops of $ZnFe_2O_4$ nanoparticles [39].

The decreasing or increasing in magnetization for any material can be attributed to the canting angle between the moments in the B-site, or and the total magnetic moments in the B-site [18]. So, the two factors may be to compete with each other and cause variation of M_s for all MF/CuAl nanocomposites. Also, the variation of M_s with the nanocomposites can be explained in light of the exchange interactions between the MF and CuAl. In other words, the combination of two different magnetic materials in which their different magnetic domains yield a new compound; the second domain may lead to a decrease or increase in the magnetization of the new compound, owing to interferences of the two magnetic domains [40].

The following equations for the determination of Bohr Magneton (m_B), magnetocrystalline anisotropy constant (K), and initial permeability (m_i) are used [41].

$$m_B = [M \times M_s] / [5585 \times r_{Xray}] \quad (5)$$

$$K = [H_c \times M_s] / 0.96 \quad (6)$$

$$m_i = [M_s^2 \times D] / K \quad (7)$$

where the M, M_s, H_c, and D are the molecular weight, magnetic saturation, coercivity, and grain size of the MF/CuAl nanocomposites. Table 4 listed the magnetic parameters such as M_s, M_r, H_c, Bohr Magneton, initial permeability, magnetic squareness, and anisotropy. The variation of M_s, M_r, H_c is due to the values of the magnetic moment of Ni^{2+}, Co^{2+}, Mg^{2+} Zn^{2+}, Cu^{2+}, Fe^{3+}, and Al^{3+} ions, which are 2.3, 3.85, 0, 0, 1.73, 5, and 0 m_B, respectively. Also, the variations in the magnetic moment of Ni^{2+}, Co^{2+}, Mg^{2+} Zn^{2+}, Cu^{2+}, Fe^{3+}, and Al^{3+} ions are responsible for the variations in the magnetocrystalline anisotropy, Bohr Magneton, magnetic domain, and super exchange interactions. The coercive field generally decreases with particle size decrease because of lower anisotropy barriers [29]. A similar dependence of coercivity on the variations of the magnetic moment is reported in other works [42, 43].

3.3.3 Magnetic hyperthermia

The specific power absorption rate (SAR) values of the magnetic suspended solution were calculated using the Eq. [15]

$$SAR = 1307\sqrt{\frac{k}{m}} \quad (8)$$

where C_i and M_i are the specific heat and the mass component, i of the system, respectively, M_{Fe} the mass of the magnetic component and (DT/Dt) the initial heating rate. The (DT/Dt) was taken from the initial heating part of the curves in Fig. 8. The heating effect, due to the external magnetic field applied to the investigated samples, was measured with time starting from switching the power on the induction coil. The obtained values were represented by curves of temperature as a function of time. As seen from the figure, the NiF/CuAl has less time to reach the hyperthermia temperature as compared to the other samples.

Fig. 9 and Table 4 show the SAR values of MF/CuAl samples. The presented graphs revealed that the highest SAR effect was obtained for the NiF/CuAl sample while CoF/CuAl was the lowest. The MgF/CuAl and ZnF/CuAl are intermediate. Despite the CoF/CuAl sample is the highest value of magnetization, i.e., magnetic moment perturbation in the magnetic field, the value of the SAR is lower than that of NiF/CuAl and MgF/CuAl. These results can be explained according to Neel and Brownian relaxations [44, 45]. It is known that the magnetic anisotropy constant is directly proportional to magnetic coercivity. Hence, the

heat generation process which governed by both Neel and Brownian relaxations rather than M_s. Thus, the SAR always decreases if H_c increase. The heating curves of the MF/CuAl, samples indicate that the NiF and MgF have a very significant effect on the SAR parameter.

Conclusion

According to the XRD combination between MF (=$NiFe_2O_4$, $CoFe_2O_4$, $MgFe_2O_4$, and $ZnFe_2O_4$) with $CuAl_2O_4$ was successfully synthesized to form multiferroic nanocomposites, which are considered brand-new nanocomposites. The lattice parameters of MF/CuAl nanocomposites are different from the individual MF due to the mutual effect between MF and CuAl. This mutual effect causes to decrease in the transition magnetic temperature T_c of all MF/CuAl Nanocomposites. Also from the Hyperthermia study, the NF/CuAl having maximum SAR and minimum time required to reach the desired hyperthermic temperature as compared to other samples. Thus, it is demonstrated that the combustion synthesized of NF/CuAl can be explored for potential applications in the field of biomedicine, especially in magnetic particle hyperthermia.

References

1. Yu, L. et al. Evaluation of Hyperthermia of Magnetic Nanoparticles by Dehydrating DNA. Sci. Rep. 4, 7216 (2014). DOI:10.1038/srep07216 (2014).
2. E. A. Périgo, G. Hemery, O. Sandre, D. Ortega, E. Garaio, F. Plazaola, and F. J. Teran, Fundamentals and advances in magnetic hyperthermia, Appl. Phys. Rev. 2, 041302 (2015). http://dx.doi.org/10.1063/1.4935688.
3. Diana Saykova, Svetlana Saikova, Yuri Mikhlin, Marina Panteleeva, Ruslan Ivantsov, and Elena Belova, Synthesis and Characterization of Core-Shell Magnetic Nanoparticles NiFe2O4@Au, Metals 10, 1075 (2020); https://doi:10.3390/met10081075
4. Dzmitry Kotsikau, Vladimir Pankov, Elena Petrova, Valentin Natarov, Dmitry Filimonov, Konstantin Pokholok, Structural, magnetic and hyperfine characterization of ZnxFe3–xO4 nanoparticles prepared by sol-gel approach via inorganic precursors, J. Phys. Chem. Sol. 114 64–70 (2018). https://doi.org/10.1016/j.jpcs.2017.11.004
5. Hajar Jalili, Bagher Aslibeiki, Ali Ghotbi Varzaneh, and Volodymyr A. Chernenko, The effect of magneto-crystalline anisotropy on the properties of hard and soft magnetic ferrite nanoparticles, Beilstein J. Nanotechnol. 10, 1348–1359 (2019). https://doi:10.3762/bjnano.10.133.
6. Ansari M, Bigham A, Hassanzadeh Tabrizi SA, Abbastabar Ahangar H. Copper-substituted spinel Zn-Mg ferrite nanoparticles as potential heating agents for hyperthermia. J Am. Ceram. Soc.;101:3649–3661 (2018). https://doi.org/10.1111/jace.15510
7. Sofia G. Mendo, Andre´ F. Alves, Liliana P. Ferreira, Maria Margarida Cruz, Maria Helena Mendonça, Margarida Godinho, and Maria Deus Carvalho, Hyperthermia studies of ferrite nanoparticles

synthesized in the presence of cotton, New J. Chem., 39, 7182, (2015) https://doi:10.1039/c5nj00009b.

8. Sofia G. Mendo, Andre´ F. Alves, Liliana P. Ferreira, Maria Margarida Cruz, Maria Helena Mendonça, Margarida Godinho, and Maria Deus Carvalho, Hyperthermia studies of ferrite nanoparticles synthesized in the presence of cotton, New J. Chem., 39, 7182, (2015) https://doi:10.1039/c5nj00009b.
9. S. Fayazzadeh, M. Khodaei, M. Arani, S. R. Mahdavi, T. Nizamov, and A. Majouga, Magnetic Properties and Magnetic Hyperthermia of Cobalt Ferrite Nanoparticles Synthesized by Hydrothermal Method, J Supercond Nov Magn. (2020), https://doi.org/10.1007/s10948-020-05490-6
10. Kh. Roumaih, M. Yehia, H. E. Hassan, Synthesis and Characterization of Core-Shell NiFe2O4@MgFe2O4 and ZnFe2O4@MgFe2O4 Nanoferrites, Journal of Inorganic and Organometallic Polymers and Materials 30:3132–3142 (2020). https://doi.org/10.1007/s10904-020-01476-y
11. Kh. Roumaih, 2021 *Phys. Scr.*https://doi.org/10.1088/1402-4896/ac2087.
12. M Veverka *et al*, Distribution of cations in nanosize and bulk Co–Zn ferrites, Nanotechnology 22, 345701 (2011). https://doi.org/10.1088/0957-4484/22/34/345701.
13. Lisjak D, Jenusˇ P, Mertelj A: Influence of the morphology of ferrite nanoparticles on the directed assembly into a magnetically anisotropic hierarchical structure, Langmuir, 30:6588-6595 (2014).
14. H.M. El-Sayed, I.A. Ali, A. Azzam, A.A. Sattar., Influence of the magnetic dead layer thickness of Mg-Zn ferrites nanoparticle on their magnetic properties., J. Magnetism and Magnetic Materials 424, 226–232 (2017).
15. Kh. Roumaih, Shaban I. Hussein., Effect of Ba Ion on Phase Formation, Microstructure and Photocatalytic Properties of the $CuAl_2O_4$ Nanoparticle., Eur. J. Appl. Sci., 9 212 (2021).
16. L. Lutterotti, P. Scardi, Simultaneous structure and size-strain refinement by the Rietveld method, J. Appl. Cryst. 23 246–252 (1990). http://maud.radiographema.eu.
17. Dulal C. Ghosh and Raka Biswas, Theoretical Calculation of Absolute Radii of Atoms and Ions, Int. J. Mol. Sci. 4 379-407 (2003).
18. M.A. Hakim, et al., Spin-glass-like ordering in the spinel $ZnFe_2O_4$ ferrite, Physica B 406 48 (2010). DOI:10.1016/j.physb.2010.10.010.
19. H. Ehrhardta, S.J. Campbell, M. Hofmann, Structural evolution of ball-milled $ZnFe_2O_4$, J. Alloys. Compd. 339 255 (2002).https://doi.org/10.1016/S0925-8388(01)02011-4
20. C. N. Anumol, M. Chithra, Shantinarayan Rout, and Subasa C. Sahoo, Effect of Magnesium Substitution on Structural and Magnetic Properties of Nickel Ferrite Nanoparticles, J Supercon. Nov. Magn. https://doi.org/10.1007/s10948-019-05192-8
21. Yue Zhang, Yong Liu, Chunlong Fei, Zhi Yang, Zhihong Lu, Rui Xiong, Di Yin, and Jing Shi, The temperature dependence of magnetic properties for cobalt ferrite nanoparticles by the hydrothermal method, J. Appl. Phys. 108 084312 (2010).

22. John Philip, G. Gnanaprakash, G. Panneerselvam, M.P. Antony, T. Jayakumar, and Baldev Raj, Effect of thermal annealing under vacuum on the crystal structure, size, and magnetic properties of $ZnFe_2O_4$ nanoparticles, J. Appl. Phys. 102 054305 (2007).
23. Zhenfa Zi, Yuping Sun, Xuebin Zhu, Zhaorong Yang, Jianming Dai, Wenhai Song, Synthesis and magnetic properties of $CoFe_2O_4$ ferrite nanoparticles, J. Magn. Magn. Mater. 321 1251–1255 (2009). doi:10.1016/j.jmmm.2008.11.004.
24. Xuan Guo, Haojun Zhu, Mingsu Si, Changjun Jiang, Desheng Xue, Zhihua Zhang, and Quan Li, $ZnFe_2O_4$ Nanotubes: Microstructure and Magnetic Properties; The Journal of Physical Chemistry; 118, 51, 30145-30152 (2014). https://doi.org/10.1021/jp507991e.
25. Yan Xu, Yantian Liang, Lijuan Jiang, HuaruiWu, Hongzhi Zhao, and Desheng Xue; Preparation and Magnetic Properties of $ZnFe_2O_4$ Nanotubes; Journal of Nanomaterials; Volume 2011, Article ID 525967, 5 pages (2011). https://doi:10.1155/2011/525967.
26. Waldron RD. Infrared spectra of ferrites, Phys. Rev.99 1727 (1955).
27. R. S. Patil, S. V. Kakatkar, A. M. Sankpal, S. R. Sawant, Indian, J. Pure Appl. Phys. 32 193 (1994).
28. H. M. Zaki, H. A. Dawoud, Physica B 405 4476 (2010).
29. A. D. Cross, R. A. Jones, “Introduction to Practical Infrared Spectroscopy” Butterworths, London, 3rd edition (1969).
30. J. M. D. Coey, Magnetism, and Magnetic Materials, Cambridge University Press, New York (2010). https://doi.org/10.1017/CBO9780511845000.
31. S. Manjura Hoque, M. A. Hakim, Indrijit Saha, and Per Nordblad, Effect of grain size on Neél temperature, magnetic and electrical properties of $NiFe_2O_4$ nanoparticle synthesized by chemical co-precipitation technique, NSTI-Nanotech, ISBN 978-1-4398-3401-5 Vol. 1, 518-521 (2010)
32. Naglaa M. Sadik, A. A. Sattar, M. M. Rashad, H. M. Elsayed, Physical, magnetic, and enhanced electrical properties of $SrTiO_3$–$MgFe_2O_4$ nanocomposites, SN Applied Sciences 2 620 (2020). https://doi.org/10.1007/s42452-020-2450-8.
33. A. Franco, F.L.A. Machado, V.S. Zapf, Magnetic properties of nanoparticles of cobalt ferrite at high magnetic field, J. Appl. Phys. 110, 053913 (2011). https://doi.org/10.1063/1.3626931
34. A. Franco Jr, F.L.A. Machado, V.S. Zapf, F. Wolff-Fabris, Enhanced magnetic properties of Bi-substituted cobalt ferrites, J. Appl. Phys. 109, 07A745 (2011). https://doi.org/10.1063/1.3565406
35. R. Topkaya, U. Kurtan, A. Baykal, H. So¨zeri, M. S. Toprak, Polymer Assisted Co-precipitation Synthesis and Characterization of Polyethylene Glycol (PEG)/$CoFe_2O_4$ Nanocomposite, J Inorg Organomet Polym 23:592–598 (2013). https://doi/10.1007/s10904-012-9818-1.
36. A. Alarifi, N.M. Deraza, S. Shaban, Structural, morphological and magnetic properties of $NiFe_2O_4$ nanoparticles, J. Alloys and Compounds 486 501–506 (2009).
37. A. Tomitaka, H. Kobayashi, T. Yamada, M. Jeun, S. Bae, Y. Takemura, Magnetization, and self-heating temperature of $NiFe_2O_4$ nanoparticles measured by applying ac magnetic field, Journal of Physics:

Conference Series 200 122010 (2010). DOI:10.1088/1742-6596/200/12/122010

38. C.N. Anumol, M. Chithra, M. Govindaraj Shalini, S.C. Sahoo, Effect of annealing on structural and magnetic properties of $NiFe_2O_4/ZnFe_2O_4$ nanocomposites. J. Magn. Magn. Mater. 469, 81–88 (2019). https://doi.org/10.1016/j.jmmm.2018.08.036.
39. M. Bohra, S. Prasad, N. Venkataramani, S.C. Sahoo, N. Kumar, R. Krishnan, Low-temperature magnetization studies of nanocrystalline Zn-ferrite thin films. IEEE Trans. Magn. **49**, 4249 (2013). https://doi.org/10.1109/TMAG.2013.22399 69.
40. Fashen Li, Haibo Wang, Li Wang, Jianbo Wang Magnetic properties of $ZnFe_2O_4$ nanoparticles produced by a low-temperature solid-state reaction method. *J. Magn. Magn. Mater.309*, 295-299 (2007). https://doi.org/10.1016/j.jmmm.2006.07.012.
41. Alessandra Quarta, Clara Piccirillo, Giacomo Mandriota and Riccardo Di Corato, Nanoheterostructures (NHS), and Their Applications in Nanomedicine: Focusing on In Vivo Studies, Materials 12, 139 (2019); DOI:10.3390/ma12010139.
42. M.N. Akhtar, M.A. Khan, M. Ahmad, M.S. Nazir, M. Imran, A. Ali, A. Sattar, G.Murtaza, Evaluation of structural, morphological and magnetic properties of CuZnNi($Cu_xZn_{0.5-x}Ni_{0.5}Fe_2O_4$) nanocrystalline ferrites for core, switching and MLCI's Applications, J. Magn. Magn. Mater. 421 260–268 (2017).
43. A. Ghasemi, M. Mousavinia, Structural and magnetic evaluation of substituted $NiZnFe_2O_4$ particles synthesized by conventional sol-gel method, Ceram. Int. 40 2825–2834 (2014).
44. Majid Niaz Akhtar, Muhammad Azhar Khan, Effect of rare-earth doping on the structural and magnetic features of nanocrystalline spinel ferrites prepared via sol-gel route, J. Mag. and Mag. Mat. 460 268–277 (2018). https://doi.org/10.1016/j.jmmm.2018.03.069.
45. G. Vallejo-Fernandez *et al.*, Mechanisms of hyperthermia in magnetic nanoparticles, *J. Phys. D, Appl. Phys.*, vol. 46, no. 31, p. 312001 (2013).
46. R. Rosensweig, Heating magnetic fluid with an alternating magnetic field, J. Magn. Magn. Mater. 252 370 (2002).

Tables

Table 1:**The XRD parameters of MF/CuAl nanocomposites.**

Sample	S	Phase concentration	(%)	*a* (Å)	r x-ray g/cm^3	D (nm)	Z (nm)
CoF/CuAl	1.06	$CuAl_2O_4$	0.209	8.074	9.38	80.4	25
		$CoFe_2O_4$	0.791	8.385		31	
NiF/CuAl	1.06	$CuAl_2O_4$	0.263	8.080	9.40	21.4	27
		$NiFe_2O_4$	0.737	8.376		28	
MgF/CuAl	1.08	$CuAl_2O_4$	0.342	8.074	8.63	28.3	45
		$MgFe_2O_4$	0.658	8.373		11.88	
ZnF/CuAl	1.07	$CuAl_2O_4$	0.344	8.089	9.33	26.9	25
		$ZnFe_2O_4$	0.656	8.443		13.62	

Table 2: Comparative between our work and other works.

Sample	*a* (Å) our work	*a* (Å) Other works	Ref.
$CuAl_2O_4$	8.074	8.076	17
$CoFe_2O_4$	8.385	8.396	25
$CuAl_2O_4$	8.080	8.076	17
$NiFe_2O_4$	8.376	8.337	24
$CuAl_2O_4$	8.074	8.076	17
$MgFe_2O_4$	8.373	8.376	24
$CuAl_2O_4$	8.089	8.076	17
$ZnFe_2O_4$	8.443	8.445 8.449	22 23

Table (3): IR absorption band (n_t) and the force constant (k_t)

Samples	n_t (cm^{-1})	k_t x 10^5 dynes/cm^2
ZnF/CuAl	528	7.63
MgF/CuAl	541	8.01
CoF/CuAl	547	8.18
NiF/CuAl	549	8.24

Table 4:**Magnetic parameters of MF/CuAl nanocomposites.**

Parameter	CoF/CuAl	NiF/CuAl	MgF/CuAl	ZnF/CuAl
T_C (K)	462	561	438	-
q (K)	539	566	402	-
C_M	133.5	0.333	0.172	-
m_{eff} (B.M.)	32.7	1.63	1.17	-
M_s ($emu.g^{-1}$)	46	30.68	9.36	5.7
M_r ($emu.g^{-1}$)	21.839	9.0962	1.7978	0.41312
M_r/M_s	0.474761	0.2934258	0.199756	0.0724772
H_c (G)	1349	171	128	64
K ($J.m^{-3}$)	64639.58	5464.875	1248	380
Initial permeab. (m)	0.818384	4.3059649	3.159	2.1375
Bohr magn. (m_B)	0.36539	0.2430405	0.074086	0.0462245
D (nm)	27	25	45	25
SAR ($W.g^{-1}$)	3.97	52.9	14.04	5.6

Figures

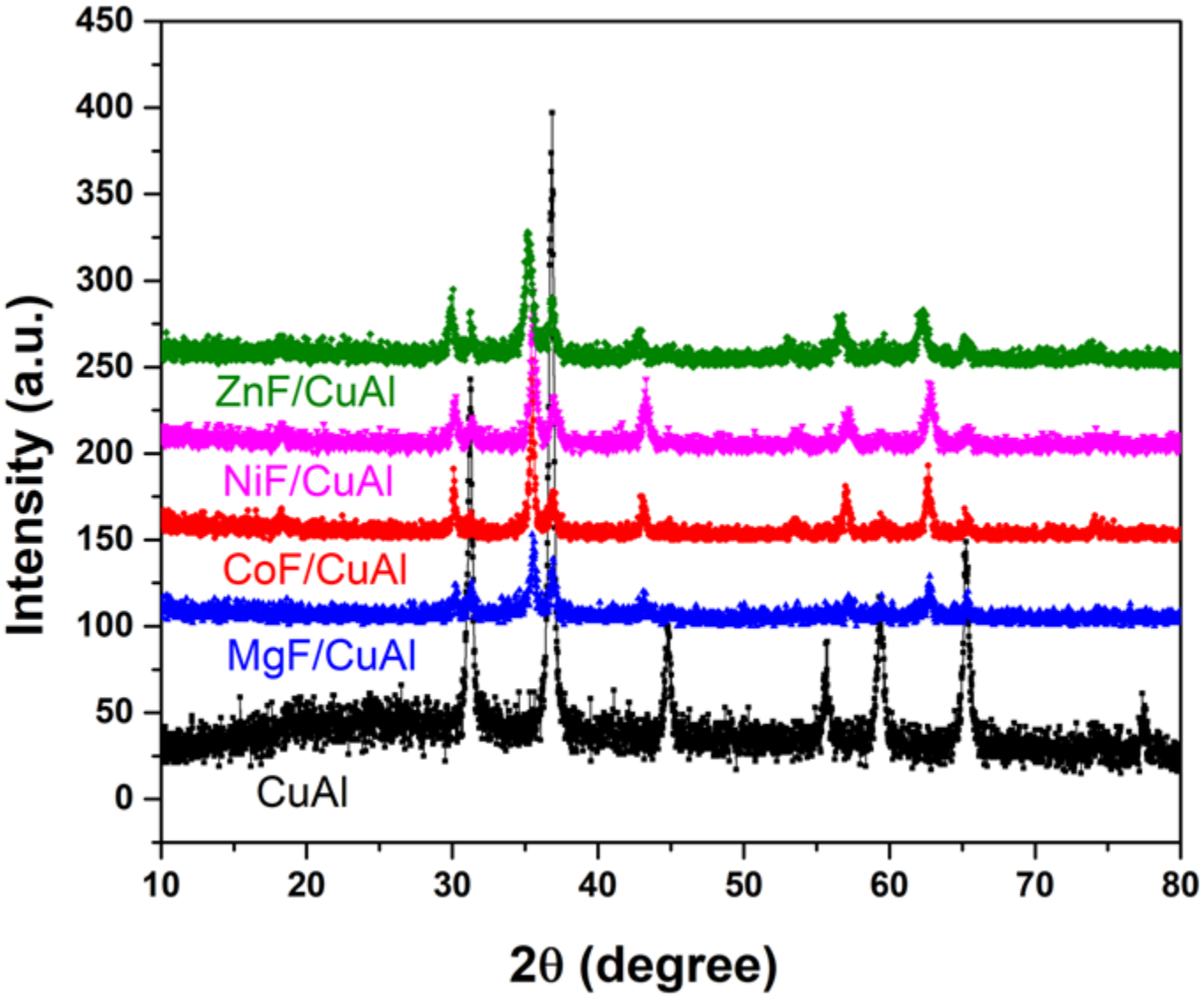

Figure 1

XRD diffraction for all MF/CuAl nanocomposite.

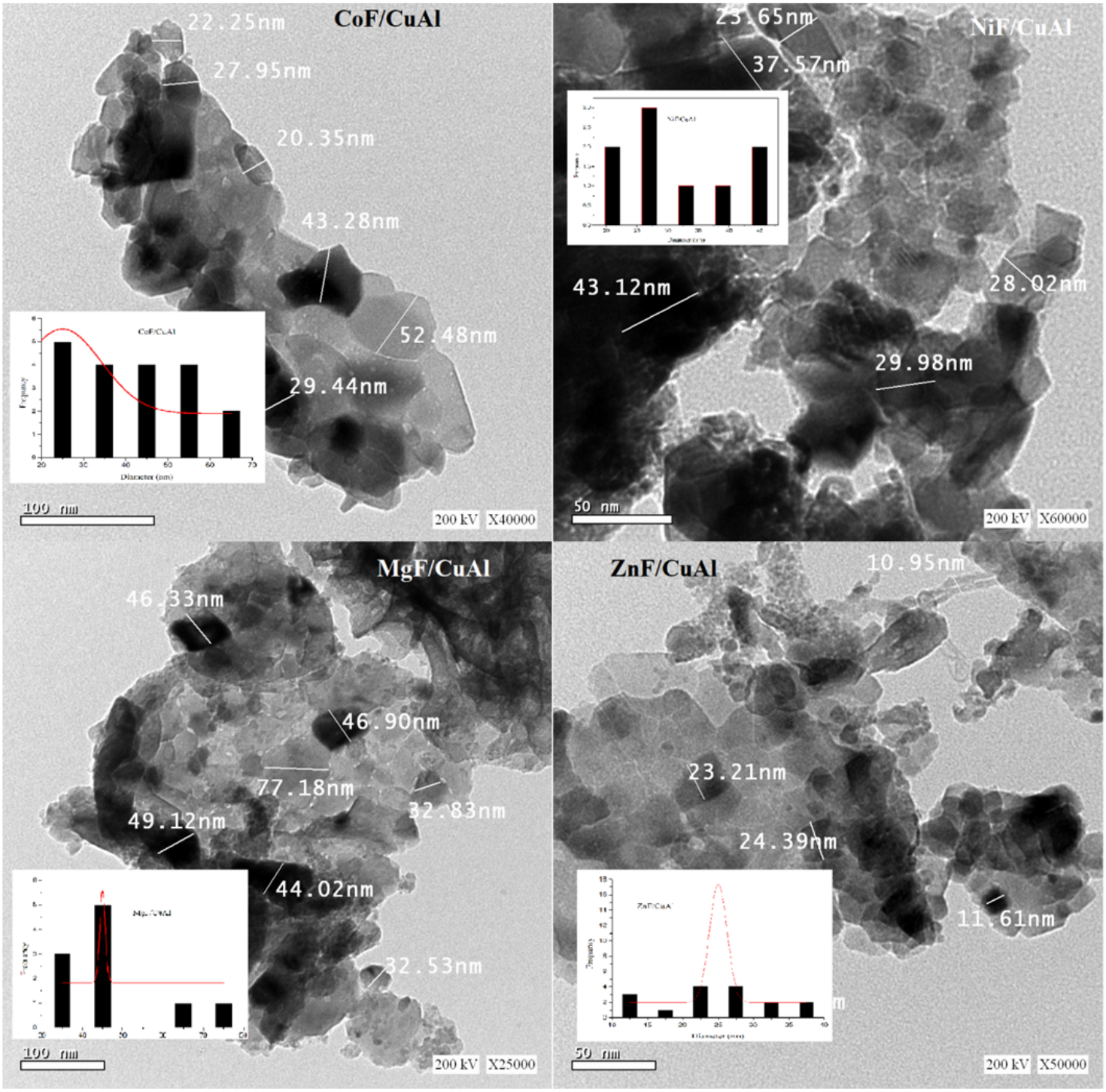

Figure 2

TEM images for all MF/CuAl nanocomposite with inset the histogram of the particle size

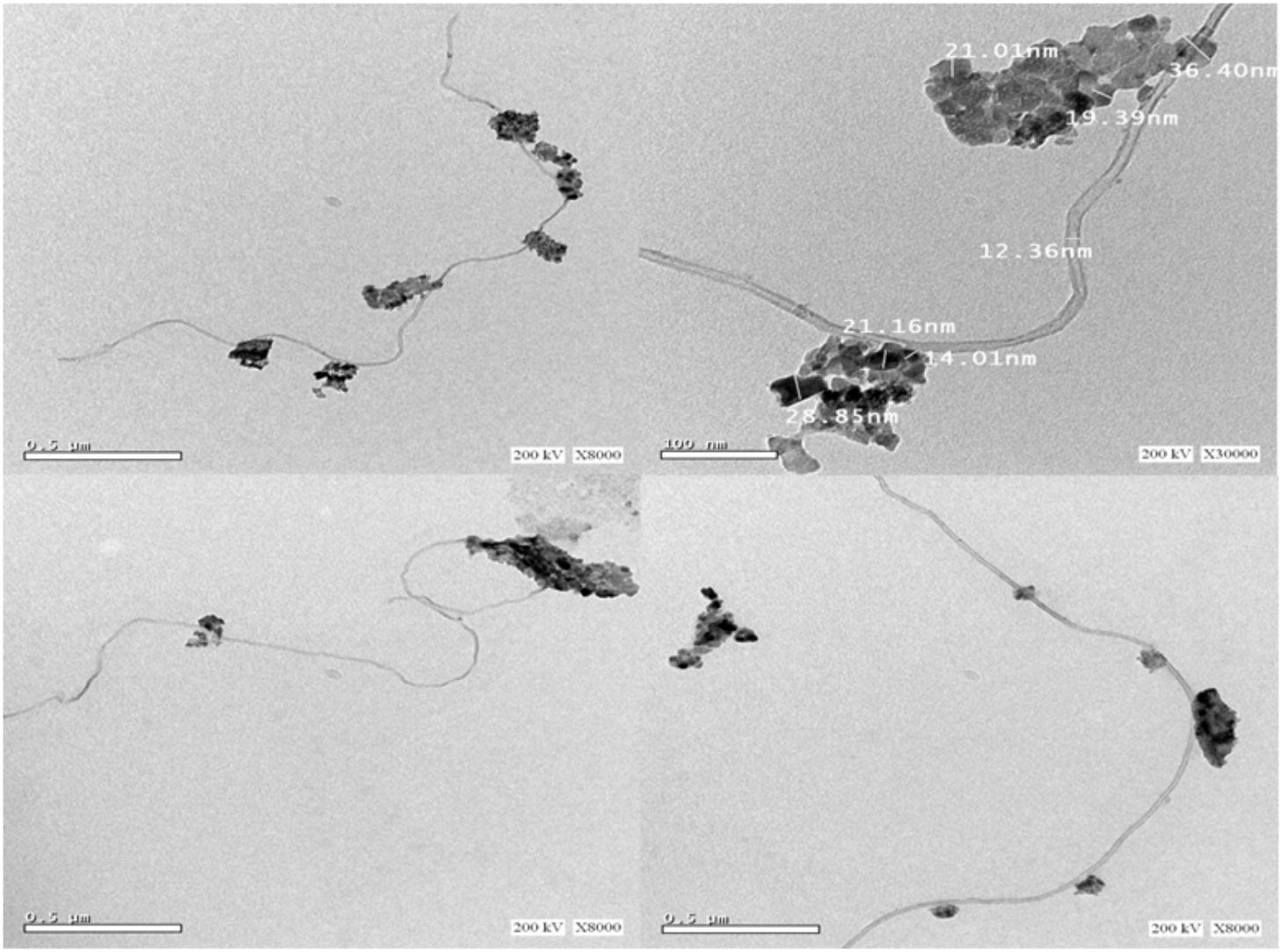

Figure 3

TEM image of a long single nanotube for ZnF/CuAl.

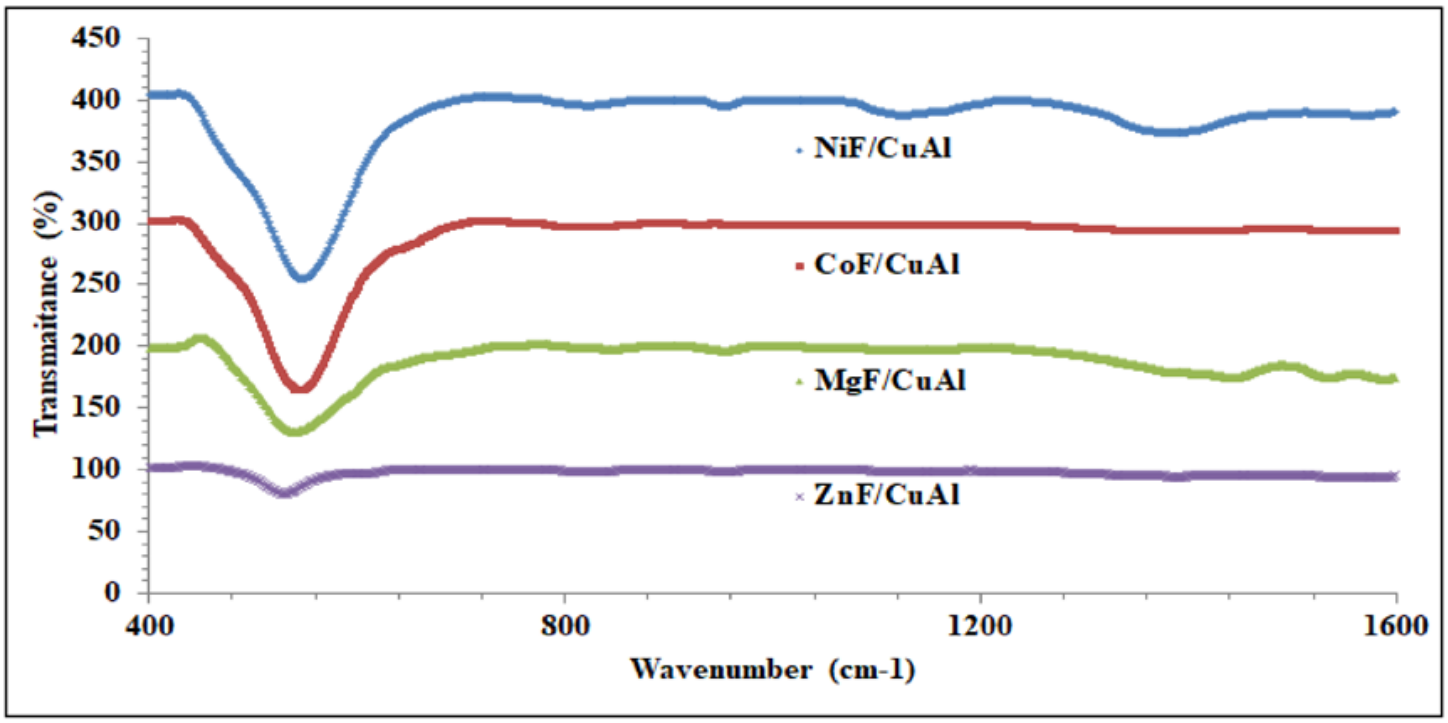

Figure 4

The IR spectra for the MFe2O4/CuAl2O4 nanocomposite

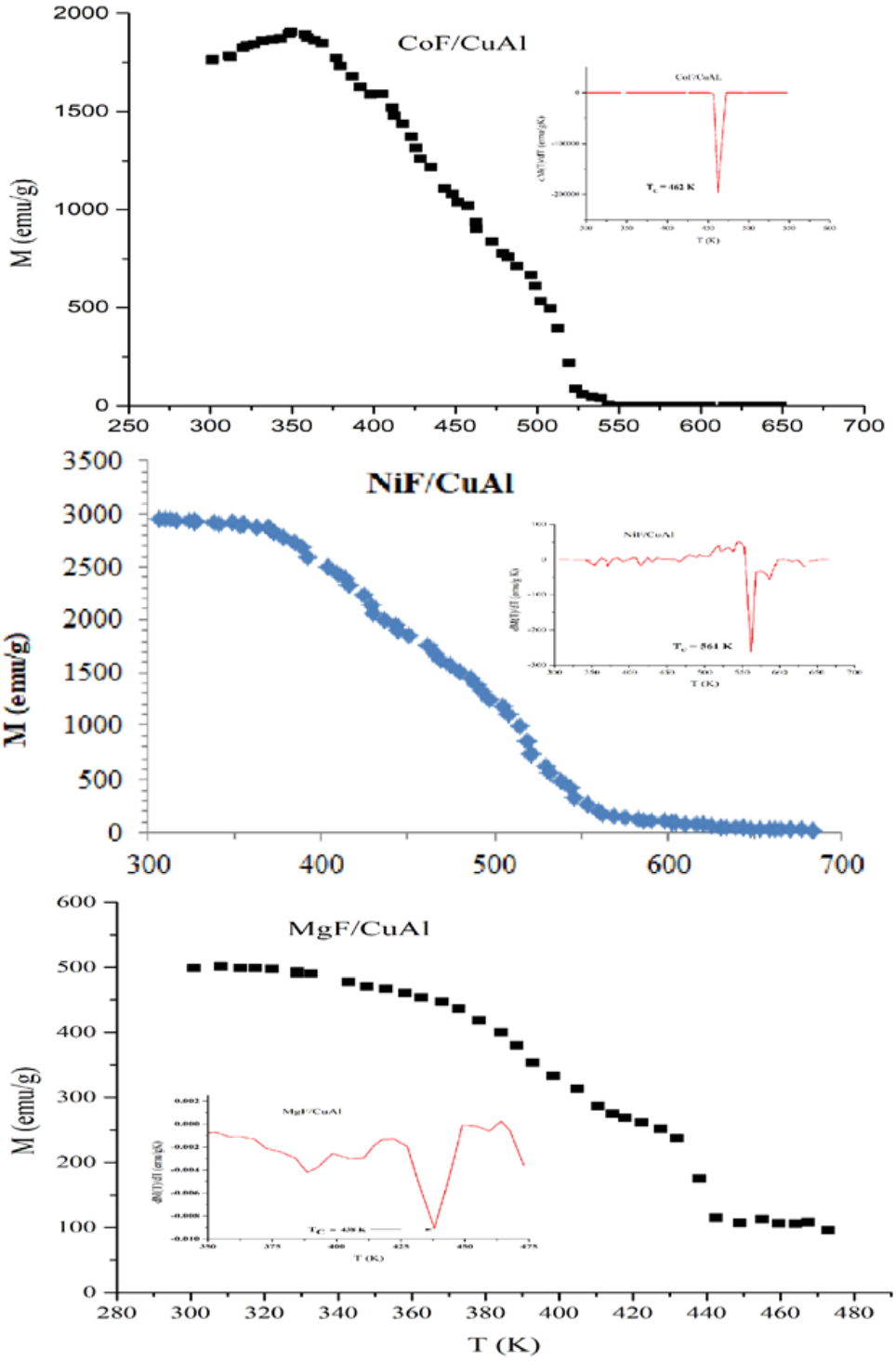

Figure 5

Magnetization versus temperature curve for all MF/CuAl nanocomposite. The inset is the temperature dependence of the first derivative of M(T)

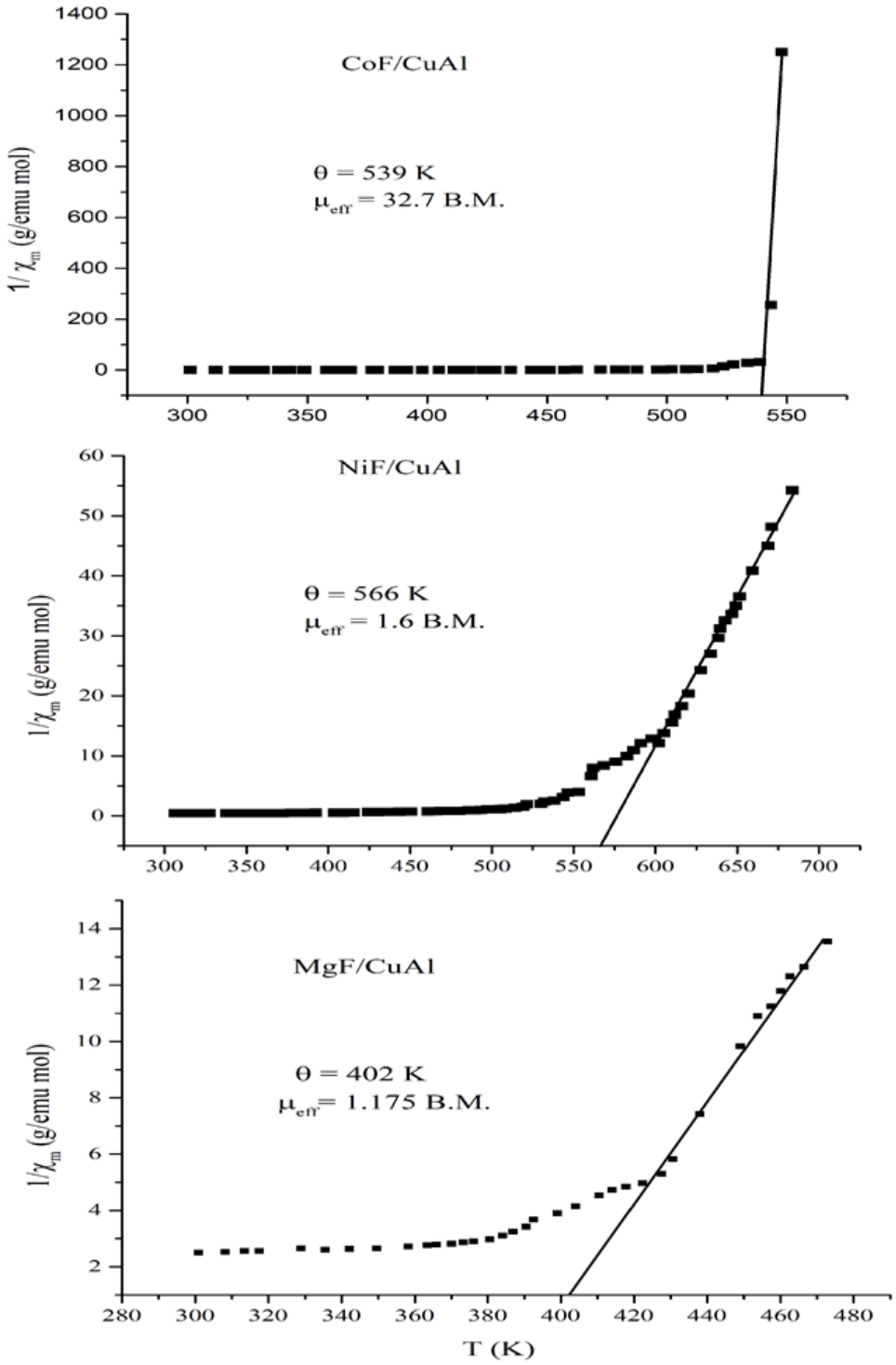

Figure 6

Temperature dependence of the χm-1 for all MF/CuAl nanocomposite

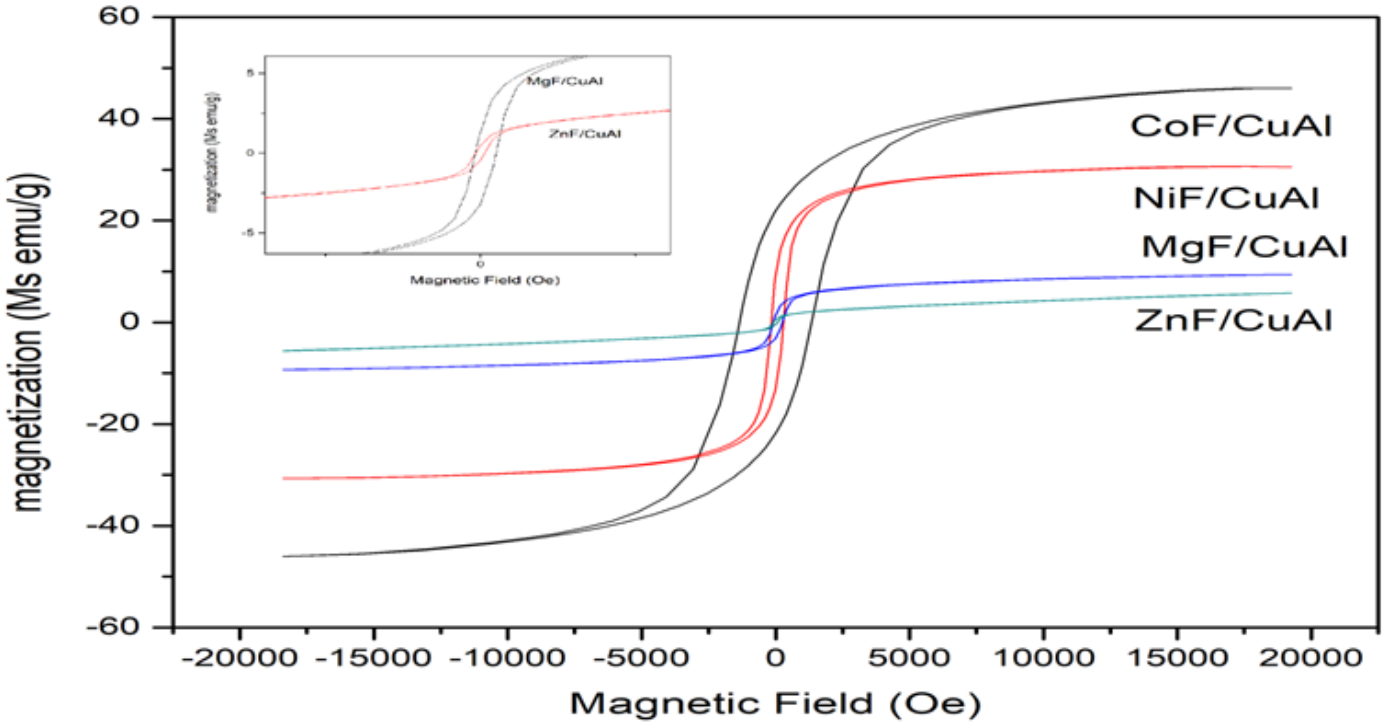

Figure 7

Hysteresis loops for the MF/CuAl nanocomposite.

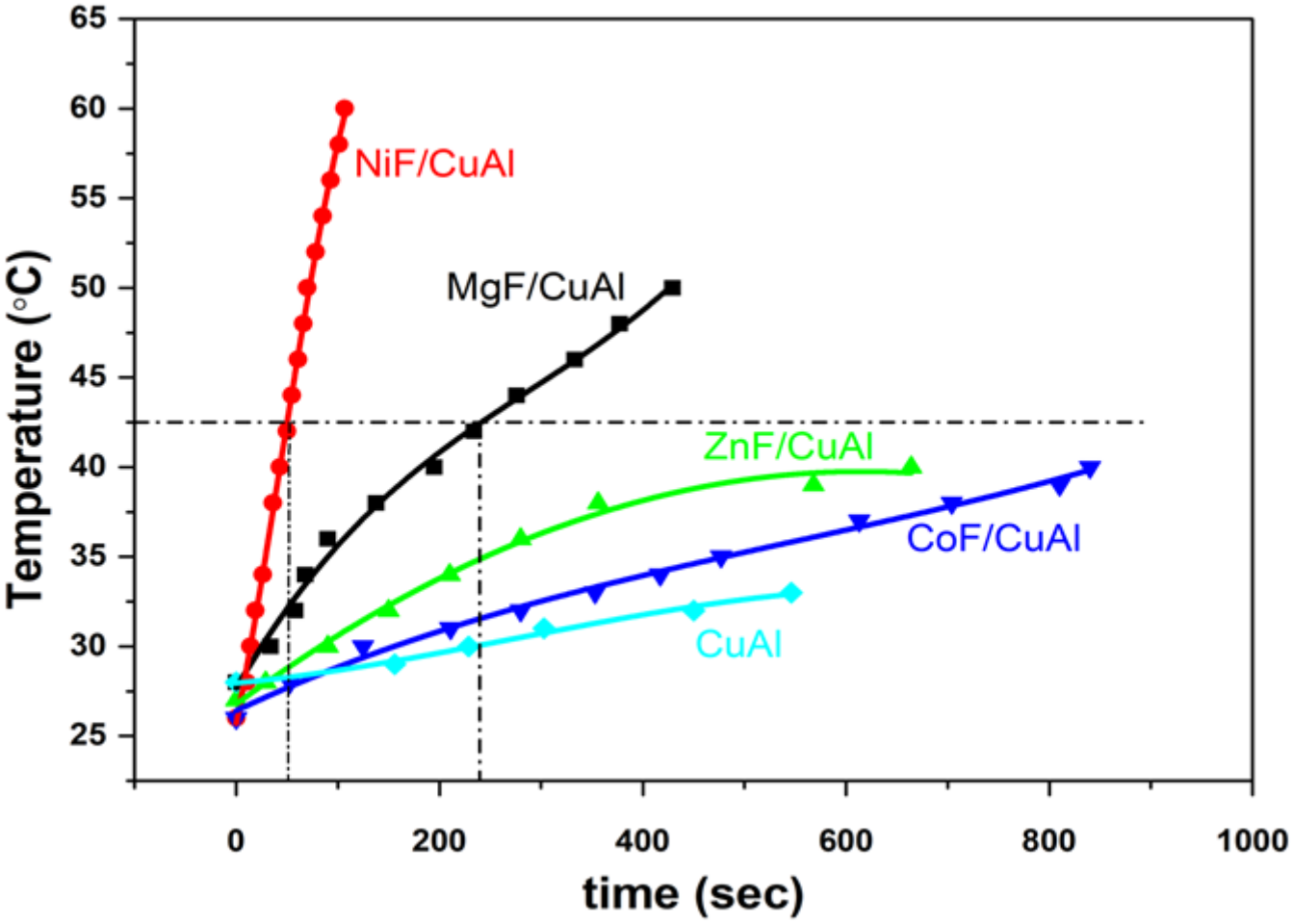

Figure 8

The temperature as a function of time (SAR) for all MF/CuAl2O4 nanocomposites.

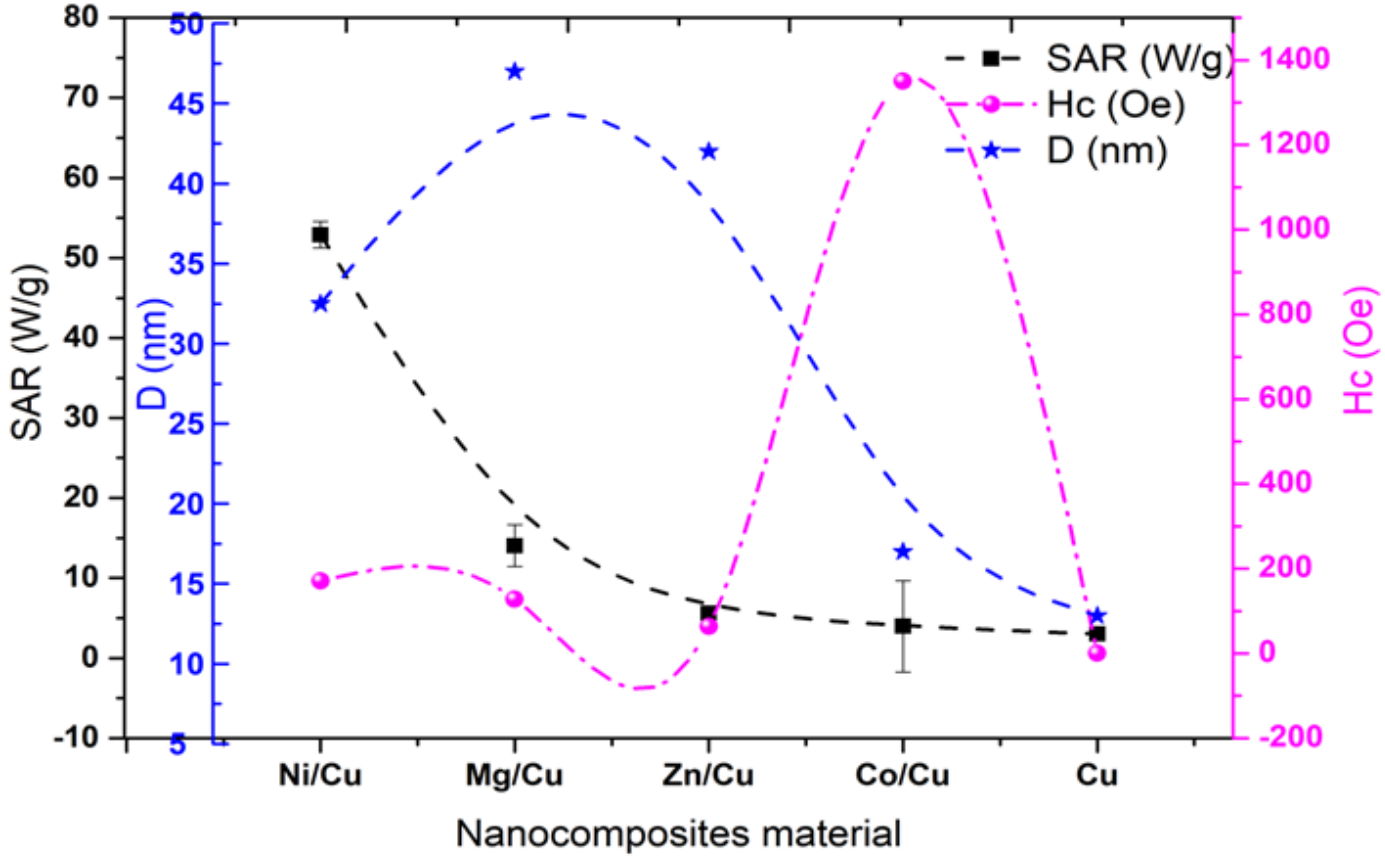

Figure 9

the relation between SAR behavior, coercive field (Hc), and the particle size (D) vs. MF/CuAl and CuAl materials.